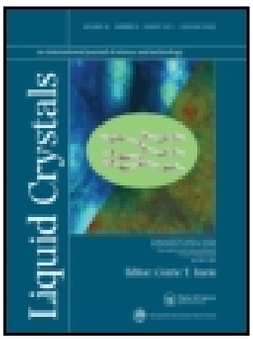

Liquid Crystals

ISSN: 0267-8292 (Print) 1366-5855 (Online) Journal homepage: https://www.tandfonline.com/loi/tlct20

Comparison of STED, confocal and optical microscopy of ultra-short pitch cholesterics

J. Pišljar, G. Posnjak, S. Pajk, A. Godec, R. Podlipec, B. Kokot & I. Muševič

To cite this article: J. Pišljar, G. Posnjak, S. Pajk, A. Godec, R. Podlipec, B. Kokot & I. Muševič (2020): Comparison of STED, confocal and optical microscopy of ultra-short pitch cholesterics, Liquid Crystals, DOI: 10.1080/02678292.2019.1710870

To link to this article: https://doi.org/10.1080/02678292.2019.1710870

Published online: 08 Jan 2020.

Submit your article to this journal

Article views: 61

View related articles

View Crossmark data

Full Terms & Conditions of access and use can be found at
https://www.tandfonline.com/action/journalInformation?journalCode=tlct20

LIQUID CRYSTALS
https://doi.org/10.1080/02678292.2019.1710870

Taylor & Francis
Taylor & Francis Group

Check for updates

Comparison of STED, confocal and optical microscopy of ultra-short pitch cholesterics

J. Pišljar[a], G. Posnjak[a], S. Pajk[a,b], A. Godec[b], R. Podlipec[a,c], B. Kokot[a] and I. Muševič[a,d]

[a]Department of Condensed Matter Physics, Jožef Stefan Institute, Ljubljana, Slovenia; [b]Faculty of pharmacy, University of Ljubljana, Ljubljana, Slovenia; [c]Ion Beam Center, Helmholz Zentrum Dresden Rossendorf, Dresden, Germany; [d]Faculty of mathematics and physics, University of Ljubljana, Ljubljana, Slovenia

ABSTRACT

The goal of this work is to compare experimentally achievable resolution limits of three different optical microscopy techniques in chiral nematic liquid crystals: (i) standard optical polarisation microscopy, (ii) confocal optical microscopy using fluorescently labelled liquid crystal and (iii) Stimulated Emission Depletion (STED) microscopy using custom synthesised fluorescent dyes. The microscopy experiments on micrometre thin LC samples reveal that the lateral resolution better than ~90 nm can be achieved using STED technique in thin layers of liquid crystals. The standard optical microscopy with index matching between the objective and the sample cover glass in combination with short-wavelength narrow-band optical illumination is quite competitive to STED technique and optical details as small as ~150 nm could be resolved using aberration limited microscope.

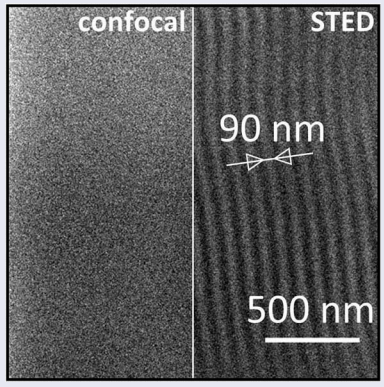

ARTICLE HISTORY
Received 3 December 2019
Accepted 29 December 2019

KEYWORDS
Sections; STED; optical microscopy; confocal microscopy; lateral resolution; short pitch cholesteric; fingerprint texture

1. Introduction

Topological defects and textures of liquid crystals, liquid crystal dispersions and liquid crystal colloids have been a subject of intense studies in the last two decades [1]. This interest was mainly driven by the extraordinary richness of fundamental topological phenomena observed in nematic and chiral nematic liquid crystals with or without inclusions. Defects and textures of liquid crystals are usually studied using polarised optical microscopy, which is limited to 2D images and finite optical resolution. The application of new microscopy methods, such as the Fluorescent Confocal Polarisation Microscopy (FCPM) [2], opened new and fascinating insight into the 3D director structures that could be visualised and reconstructed in amazing detail. Yet there is another class of super-resolution microscopies, which have not yet been studied in great detail in LCs. This includes Stimulated Emission Depletion (STED) microscopy, which is a variant of fluorescent microscopy. There are only a few studies of STED microscopy in LCs [3,4] and a single study of STED effect and its efficiency in the nematic and smectic-A liquid crystal [5]. It is therefore in the interest of liquid crystal community to compare the advantages, drawbacks and the practically achievable resolution of STED microscopy with standard optical and fluorescent microscopy when imaging structures and defects in liquid crystals.

In polarised light microscopy, the acquired image is a result of phase and amplitude contrast of birefringent sample under observation. Although LC director fields are most often observed using polarised light microscopy, fluorescent imaging methods often prove as beneficial

CONTACT J. Pišljar jaka.pisljar@ijs.si

© 2020 Informa UK Limited, trading as Taylor & Francis Group

because of their different principle of operation. In contrast to ordinary light microscopy, fluorescence microscopy acquires image of the sample by exciting fluorescent molecules in the sample to radiate fluorescent light. In this case, fluorescent dye molecules which are designed to align their radiative moment along (or perpendicular) to the local director, are added in small amounts to the LC. Since excitation of the anisotropic dye molecule is dependent on the polarisation of the excitation beam, the fluorescent emission intensity distribution is anisotropic and the amount of acquired fluorescent light depends on the local alignment of the radiative dipole moment [2]. This contrast in fluorescent light is used to acquire an image of the sample in fluorescent microscopy and it is quite clear that the image contrast depends on the degree of ordering of dye molecules with respect to the director.

FCPM uses polarised excitation and detected fluorescent light. It was successfully used to observe director fields of defects in Grandjean-Cano geometry [6], fingerprint and Schlieren structures [7], structures in twist grain boundary phases [8] and Hopf fibrations and torons [9,10]. Recently, the combination of raw FCPM data and simulated annealing algorithm was used for full three-dimensional reconstruction of complex topological structures inside chiral nematic droplets by Posnjak et al. [11–13].

The lateral resolution r_{lat} of the FCP microscope is $r_{\mathrm{lat}}^{\mathrm{conf}} = 0.44\lambda/\mathrm{NA}$ which is only slightly improved compared to Abbe's resolution limit of an optical microscope, $r_{\mathrm{lat}}^{\mathrm{opt}} = 0.5\lambda/\mathrm{NA}$. Here, λ is the wavelength of observation, NA is the numerical aperture of the objective $n \sin\theta$ and n is the index of refraction of the medium. The real improvement of confocal microscopy is in the axial or z direction $r_{\mathrm{z}}^{\mathrm{conf}}$, in which the pinhole rejects the out-of-focus light coming from the sample giving $r_{\mathrm{z}}^{\mathrm{conf}} = 1.5n\lambda/\mathrm{NA}^2$ [14]. In addition to fundamental limitations, the imaging resolution of polarised and fluorescence microscopy is deteriorated by polarisation properties of birefringent LC samples, leading to often complex light propagation that involves lensing effects, polarisation guiding, etc. [15]. Practically obtained resolution of FCPM imaging in real LC samples is typical of the order of 300 nm in the lateral direction (i.e. within the imaging plane), whereas the resolution along the optical axis (i.e. the z-axis) is of the order of 600 nm [16].

STED microscopy uses a method of manipulating fluorescence that has been developed in the 1990s by Stefan Hell [17,18] and is able to surpass the classical diffraction limit. The lateral resolution of the FCP microscope is significantly improved when the excitation light pulse (tens to hundreds of picoseconds duration) of a Gaussian-shaped beam is followed by a pulse (hundreds of pico- to nanoseconds) of a red-shifted doughnut-shaped beam before the spontaneous fluorescent emission takes place. This doughnut beam (also called STED or depletion beam) is usually tuned towards the far-red tail of the dye emission spectra to ensure sufficient stimulated emission while decreasing the probability for excitation of the dye molecules by this higher intensity beam. Because this doughnut beam is dark in the centre, the process of stimulated emission takes place only in the bright rim of the doughnut, whereas the centre remains excited. While the stimulated emission takes most of the energy from the excited dye molecules away from the photodetector, this photodetecor collects at a later time (nanoseconds) fluorescently emitted light from the non-depleted area of the sample. The diameter of this non-depleted area is much smaller than the theoretical Abbe's diffraction limit and is of the order of tens of nanometres. This is the core idea of STED microscopy, which acquires fluorescent images below the "classical" resolution limit. The non-depleted area reduces with increasing STED beam intensity I_{STED}, meaning the resolution is crucially determined by I_{STED}. It was shown theoretically that in case of STED microscopy the Abbe expression for the resolution is extended to [18]

$$r_{\mathrm{STED}} \approx \frac{\lambda}{2\mathrm{NA}} \cdot \frac{1}{\sqrt{1 + I_{\mathrm{STED}}/I_{\mathrm{sat}}}}, \tag{1}$$

where I_{sat} is the saturation intensity.

Development of STED and related super-resolution techniques was mainly driven for the application in life sciences [19–21]. There are not many reports of using optical super-resolution techniques in liquid crystals. Structures of labelled amphiphiles self-assembled in −1/2 defects with size less than 80 nm were imaged using stochastic optical reconstruction microscopy, a variant of Single-Molecule Localisation Microscopy [3]. Wider use of STED microscopy in LC systems is delayed partly due to the absence of appropriate dyes: these should be soluble in liquid crystals, align well with the director and at the same time exhibit sufficient stimulated emission depletion with STED lasers used in commercially available STED systems. One solution is to use dyes known to perform well in liquid crystals (such as Nile Red) and appropriately configure the STED system or, alternatively, custom synthesise dyes with desired properties. Recently, a custom-built STED polarising microscope was used to image separated cholesteric fingers and two-dimensional skyrmions in strong confinement and focal conic domains in smectic LCs with < 100 nm resolution [4]. Detailed description of STED principle, timings of light pulses and the effects of

STED beam intensity and wavelength can be found in a recent STED study of Nile Red dye molecule in 5CB and 8CB [5].

The idea of this paper is to compare three different optical microscopy methods that can be used to observe structures of cholesterics with very short pitch (< 500 nm): (i) polarisation optical microscopy, (ii) confocal fluorescence microscopy and (iii) STED microscopy. These three methods have been used for imaging director structures in thin layers of short-pitch cholesteric LCs, where four different values of the pitch were selected: 420 nm, 277 nm, 200 nm and 158 nm. For fluorescence confocal and STED microscopy of these samples, two dedicated STED dyes were designed and synthesised. We demonstrate that indeed STED microscopy is quite superior in spatial resolution, as we could clearly image cholesteric structures with 180 nm helical periodicity. Surprisingly, well-designed and index-matched optical microscopy using narrow band near UV LED illumination gives very high-quality images, clearly resolving structures in samples with helical period of 280 nm.

2. Experimental methods

2.1. Fluorescent probes

For STED and confocal microscopy two fluorescent dyes were designed and synthesised, SAG38 and PAG27. These are coumarin-based dyes, which have a long history of use and form the majority of commercially available fluorescent probes with large Stokes shifts. Probes SAG-38 and PAG-27 (Figure 1(a)) are derivatives of Coumarin 6, which has absorption and emission maximum in ethanol at 459 and 500 nm, respectively [22]. Therefore, modifications to the structure of Coumarin 6 were made in order to obtain dyes with spectral properties matching the requirements of STED microscope, i.e. excitation at 561 nm and STED at 775 nm. Red-shift of excitation and emission spectra was achieved by the introduction of electron-withdrawing cyano group at position 4 [23]. Additional red-shift was produced by incorporation of amino group at position 7 into 2,2,4-trimethyl-1,2-dihydroquinoline fragment [24]. The latter also

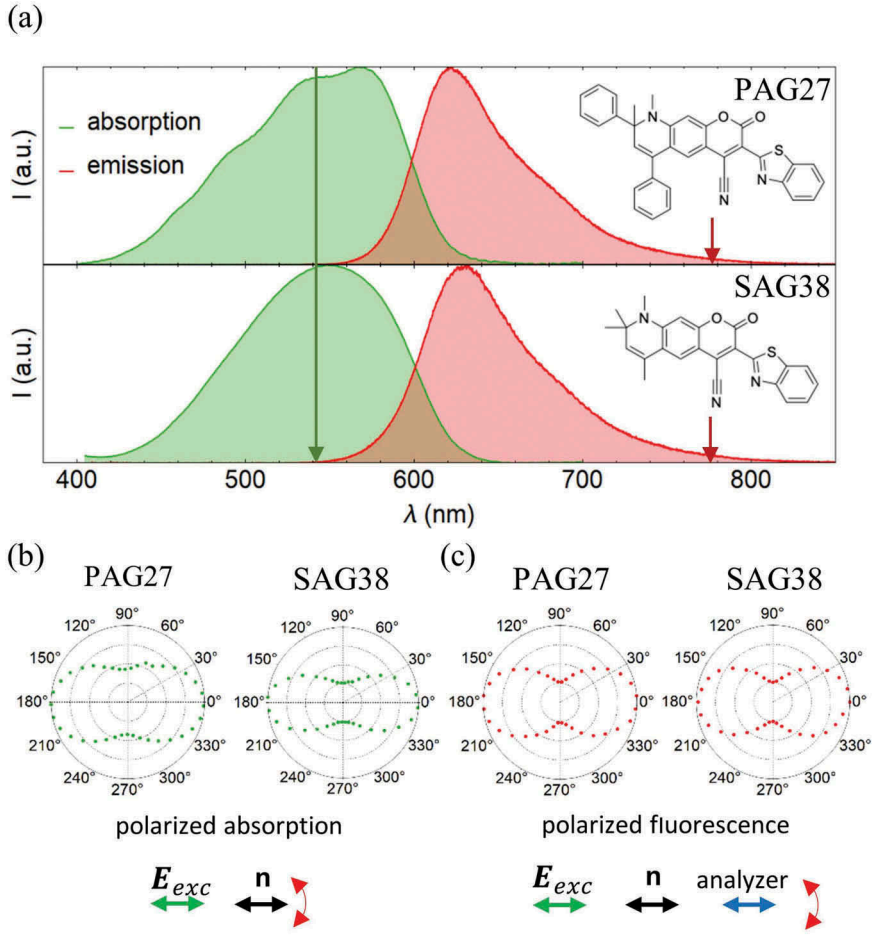

Figure 1. (Colour online) (a) Emission (red) and absorption (green) spectra of the dyes used for STED microscopy. Green and red arrows denote wavelengths of excitation and STED lasers used for our experiments. (b) Polarised absorption of PAG 27 and SAG 38 dyes. (c) Polarised fluorescence of PAG 27 and SAG 38 dyes.

provides rigidity which in turn improves fluorescence efficiency, because upon excitation the transition from intramolecular charge transfer state to non-emissive twisted intramolecular charge-transfer state is not possible [24]. Both SAG-38 and PAG-27 are highly lipophilic and practically insoluble in water. On the other hand, their planar and aromatic structure enables $\pi - \pi$ interactions, e.g. with cyanobiphenyl moiety of 5CB molecules that constitute liquid crystals. In this respect, two phenyl groups attached to 1,2-dihydroquinoline moiety of PAG-27 are able to form additional $\pi - \pi$ interactions compared to SAG-38, which has two methyl groups instead.

The absorption and emission properties of both dyes were measured in homogeneously aligned glass cells filled with dye doped 5CB (Merck KGaA, Germany). The dyes were first dissolved in acetone and then added to 5CB (Merck KGaA, Germany) in mass concentration of $\sim$ 0.1%. Both dyes show good solubility in acetone. The LC-acetone-dye mixture was homogenised by shaking and left in a closed container for 1 h. The container was opened and left at room temperature for 24 h, allowing the acetone to evaporate. Prior to usage, the LC-dye mixture was held at an elevated temperature of 80°C to completely evaporate any remaining acetone. We measured the absorption and emission spectra of unpolarised light from the glass cell filled with the fluorescent mixtures, which are shown in Figure 1(a).

To determine the angular anisotropy of the absorption and emission of the dyes and the degree of alignment of their transition dipole moments with the nematic director, we measured polarised absorption and fluorescence. The rubbed samples were excited using linearly polarised green laser (532 nm) focussed on the sample using a 20x (Nikon CFI Plan Fluor) objective. The fluorescent light was collected by the same objective and its total intensity was obtained by integrating the obtained fluorescent spectra. The polarised absorption dependence was obtained by measuring fluorescence intensity, while varying the angle between the excitation light polarisation and the sample rubbing direction. The results are shown in Figure 1(b). Conversely, polarised fluorescence, shown in Figure 1(c), was measured by fixing the angle between the polarisation and sample rubbing direction and recording the intensity of emitted light passing through a rotating analyser. Maximal fluorescence was obtained when both light polarisation ($\mathbf{E}_{exc}$) and the analyser were aligned with the sample rubbing direction ($\mathbf{n}$).

From these data we determined the degree of dye alignment, which is described by the dichroic order parameter S_ϕ

$$S_\phi = \frac{I_\parallel - I_\perp}{I_\parallel + 2I_\perp}, \tag{2}$$

Here $I_\perp$ and $I_\parallel$ are emission intensities in perpendicular and parallel configurations of the rubbing direction and (i) light polarisation in the absorption measurements and (ii) the analyser in polarised fluorescence measurements. S_ϕ can take values from −0.5 to 1, depending on the nature and the degree of dye-director alignment. In our samples, the measured S_ϕ values for absorption are 0.31 and 0.50 for PAG27 and SAG38, respectively, while the S_ϕ for fluorescence is $\approx$ 0.50 in case of both dyes.

2.2. Sample preparation

Short-pitch cholesteric samples used were mixtures of an achiral nematic BL087 (commercial cyano-biphenyl mixture, $n_o = 1.5246$, $\Delta n = 0.2362$, $T_{NI} > 90^\circ$C) and a chiral dopant R5011, both obtained from Merck KGaA, Germany [25]. For different mixtures, the concentration of the chiral dopant was varied by a few per cent to obtain pitch values from 450 nm to around 150 nm. Pitch of these mixtures used in our experiment (but without fluorescent dyes) was previously determined using Atomic Force Microscopy (AFM) [26]. Glass cells used for microscopy were prepared using two cover glasses (VWR) treated for homeotropic anchoring (octadecyldimethyl (3-trimethoxysilylpropyl) ammonium chloride (DMOAP), ABCR GmbH) by pressing a small (0.1 μl – 0.3 μl) droplet of the cholesteric mixture between them, which produced an LC layer of variable thickness d below $\sim$2 μm. The thickness of the LC layer between the glass slides was estimated using 3D STED imaging capability of our microscope.

2.3. Optical microscopy

Optical micrographs were obtained on inverted microscope (Ti-U, Nikon), operated in reflection mode using a high numerical aperture oil immersion objective (Nikon CFI Plan Apochromat Lambda 100x oil, 1.45 NA), ensuring lowest possible refractive index mismatch between the objective and the top cover-glass of the sample cell. To illuminate the sample, LED illumination system (CoolLed pE-300) was used, with selectable 400 nm or 450 nm light source with bandwidths of 20 nm and 50 nm, respectively. The images were acquired using FLIR Chameleon3 greyscale camera with 3.45 μm pixel size and 2448 × 2048 pixels. The illumination light was not polarised, thus the image contrast is due to the spatial variation of the reflection

coefficient due to spatial variation of the LC structure close to the surface. Similar technique was used in our recent studies of half-skyrmion lattice in thin layers of Blue Phase liquid crystal [27].

2.4. STED and confocal microscopy

We used a custom designed Aberrior Instruments STED microscope based on a Olympus IX83 body with Olympus UPlanSApo 60x (1.2NA) water and Olympus UPlanSApo, 100x (1.4NA) oil immersion objectives. A schematic of the used STED setup is shown in Figure 2. The fluorescent dyes were excited using a 561 nm pulsed laser (~120 ps pulses with ~15 μW average power at 80 MHz repetition), overlaid with a doughnut-shaped STED beam coming from a 775 nm pulsed laser (1.2 ns pulses with ~350 mW average power at 40 MHz). The doughnut-shaped beam was obtained by passing a Gaussian beam through a liquid crystal spatial light modulator which imprints a phase mask on the beam, shaping it for both 2D and 3D depletion of the excitation volume. Both beams are circularly polarised at the position of the sample, thus preventing any polarisation effects. The position of the carefully aligned excitation and STED beams is adjusted using the Quad galvo scanner mirrors. Typically, the *xy* pixel size was 5–15 nm and the signal was collected for 10 μs at each pixel. The fluorescent signal was collected using the same objective. The collected light travelled through an adjustable pinhole with a diameter typically set to 0.75 Airy units. The pinhole is followed by a filter cube, which reflects emitted fluorescent light in the band of 580–630 nm onto an avalanche photodiode (APD 1 in the schematic), counting the photons. When the STED beam is switched off, the microscope operates as a fluorescent confocal microscope.

3. Results and discussion

We studied four different cholesteric mixtures, which are denoted by integers 1, 2, 3 and 4. The pitch p of these mixtures has been previously determined using AFM to be 420, 277, 200 and 158 nm, respectively. The expected size of observed structures in cholesteric mixtures is $\sim p/2$. However, since we observed structures in relatively thin samples (d > 1μm), the observed size was usually slightly above the bulk value, most probably due to well- known unwinding effect of the confining surfaces on the bulk pitch value p [28–30]. The expected size of structures for mixture 2 (> 138 nm) is at the Abbe's diffraction limit for ordinary optical microscope, whereas the size of structures for mixture 3 (> 100 nm) is well below the resolution limit. Helical superstructures of cholesteric mixtures in cells with homeotropic anchoring were first imaged using a conventional optical microscope operated in reflection mode, as shown in the top row of Figure 3. To ensure best possible optical resolution, a high numerical aperture NA = 1.45 oil immersion objective was used in combination with a narrow-band illumination centred at 400 nm, which gives a theoretical Abbe's diffraction limit of ~137 nm. Using this system, it was possible to observe the in-plane cholesteric structures of mixtures 1 with helical period of 420 nm and mixture 2 with helical period of 277 nm, shown in Figure 3. Note that the half-period of mixture 2 can be clearly resolved, which corresponds to a separation of 150 nm. This means that the practical lateral resolution of our optical microscope (< 150 nm) is close to the theoretical Abbe's limit for this objective. For mixture 3, the expected half-period of the cholesteric structure is ~100 nm and thus below the Abbe's resolution limit of 137 nm for the used setup. Indeed, only hints of the periodic structure can be observed in the optical micrograph of mixture 3 in Figure 3.

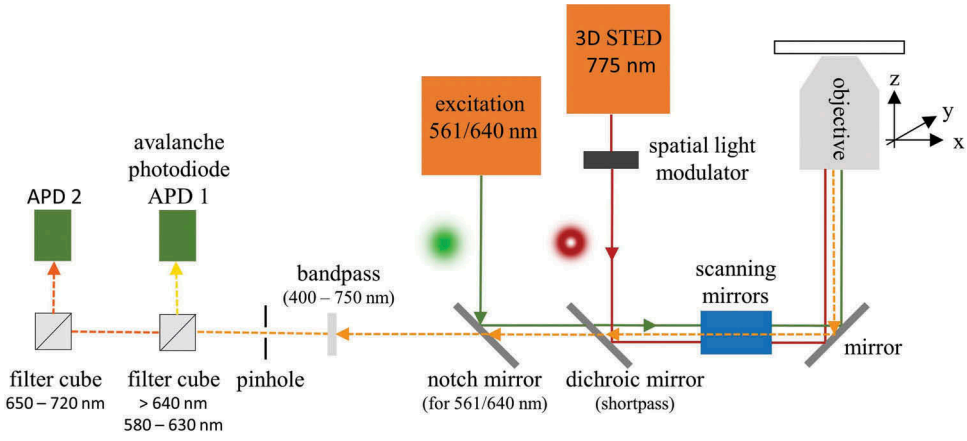

Figure 2. (Colour online) A simplified scheme of the used STED microscopy setup. APD1 is used for imaging.

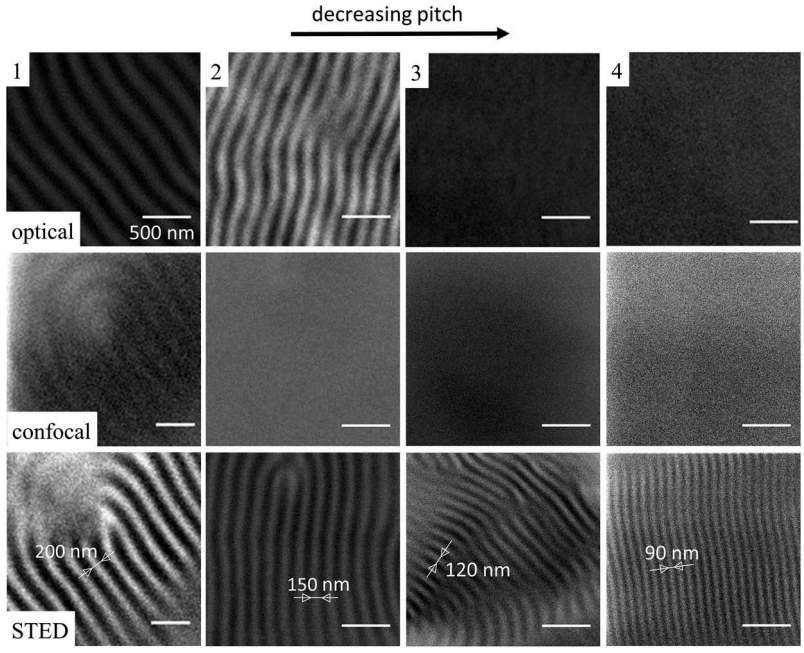

Figure 3. Comparison of three different microscopic methods of imaging structrues in short-pitch cholesterics: optical, confocal and STED microscopy. Each column corresponds to one of the four cholesteric mixtures observed with pitch decreasing with increasing label number. The helical period of mixture 1 is 420 nm, that of mixture 2 is 277 nm, of mixture 3 is 200 nm and mixture 4 has helical period of 158 nm. The scale bar corresponds to 500 nm.

For confocal microscopy and STED microscopy a circularly polarised excitation light was used, which means that no preferential direction of dye long-axis orientation within the imaging plane was selected. However, in areas where director and the aligned dye molecules are perpendicular to the imaging plane, less fluorescence is excited, because the radiating dipole of dye molecules is at nearly 90° with respect to the oscillating electric field of the excitation laser. Furthermore, since dye molecules radiate as dipolar antennas oriented along the local director the maximal fluorescence intensity in this case is also in the plane that is perpendicular to the optical axis, further decreasing signal collected from such areas [13]. As no preferential in-plane direction was chosen at detection as well, the contrast in our FCM images comes solely from the difference in fluorescent intensity of in-plane and out-of-plane dye orientations. We are interested in the lateral, *xy* resolution of the confocal system. Considering that the wavelength of the excitation laser used is 561 nm and the peak of dye emission spectra is about 650 nm we can take $\lambda_{exc} \approx \lambda_{em} \approx 600$ nm giving a value for the lateral resolution of $r_{lat}^{conf} \approx 190$ nm. This is close to the resolution limit we observed in the experiments. As can be seen from confocal images in the middle row of Figure 3, the only mixture in which any structure is observed is mixture 1 with pitch of 420 nm and half-period of 210 nm, which is slightly above the theoretical resolution limit. Note that the lateral resolution of confocal imaging is inferior to the lateral resolution of ordinary optical microscopy. The reason is in the wavelength used: in optical microscopy we use narrow-band illumination at rather short wavelength of ~ 400 nm, whereas in confocal microscopy the wavelengths used are longer. The excitation is at 561 nm, whereas the peak fluorescence is at 650 nm, which in combination gives lower resolution compared to ordinary microscopy.

Finally, we were imaging the same structures by switching-on an additional STED beam, thus transiting from confocal to STED imaging. We immediately see a significant resolution improvement compared to confocal images in all the used mixtures, as seen in the third row of Figure 3. With STED microscopy we were able to observe ULH (Uniform Lying Helix) and fingerprint-like structures in all the used mixtures. In mixture 4, where the pitch measured by AFM was 158 nm, the optical period (i.e. structural half-period) was as low as ~90 nm, giving the pitch value of 180 nm.

Spatial resolution of images of observed structures can be further enhanced by applying a spatial frequency filter to STED images, which eliminates the high-frequency noise and very low-frequency background from the acquired images. Figure 4 shows the original and filtered STED images, together with line profiles along the red lines on filtered images. From the extracted line profiles, the periodicity of observed structures can be determined

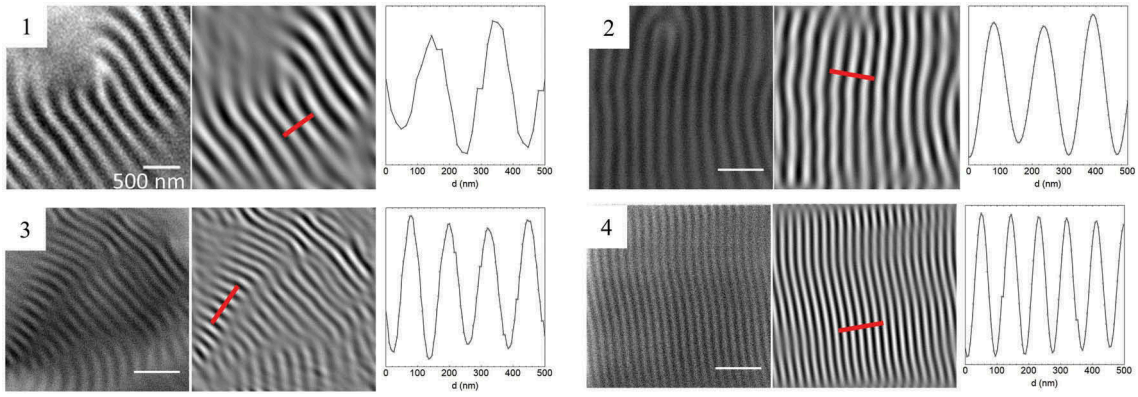

Figure 4. Comparison of line profiles for frequency filtered STED images of N* mixtures with different pitch. Since the structure of mixture 4 can be nicely resolved and the periodicity of the top green curve is ~90 nm it can be concluded that achieved resolution of our STED system is $\leq$ 90 nm.

with great accuracy. For example, helical period of the shortest pitch mixture 4 is 158 nm as determined from AFM. In optical images, the expected optical period is half a pitch, which equals to 79 nm. This half-periodicity can be clearly resolved in original and filtered images in panel 4 of Figure 4. It is equal to 90 nm and is thus slightly longer than the expected half-period of 79 nm, obtained from other samples, using AFM method. This leads to a clear conclusion that our STED resolution is slightly better than 90 nm.

It is possible to obtain STED nanoscopic resolution also in the vertical cross section of the observed cholesteric structures. Since cholesteric layers within our samples have a layer normal to the *z* axis of observation, good resolution in the *xy* direction is desirable. In Figure 5, we show STED images of structures in *xy* plane and below corresponding structures in the *xz* plane, where the central plane of the above *xy* structure is shown. It should be noted that the images of the cross sections are very sensitive to accurate alignment of the excitation and depletion beams in STED microscope. This means that the centres of the STED beams should be precisely centred to the centre of the objective to minimise any skewness of the image of the cross-sections. One can see from the cross-sections in Figure 5 that optical periodicity is the same throughout the vertical cross section and there is no visible difference between the periodicity close to the surface and the interior of the sample, as observed in some experiments in thin CLC samples [29,30]. This may be a consequence of the too small contrast differences between the two consecutive stripes.

4. Conclusion

Application of new techniques to the study of structures of liquid crystals requires precise analysis of the benefits and drawbacks of new method. While FCPM combined with reconstruction algorithms can offer direct information about the director orientation regardless of the sample birefringence [13], it is limited by the achievable resolution. In our case, where thin layers of cholesteric LC are concerned, there is no doubt that STED microscopy significantly improves the lateral resolution of the confocal

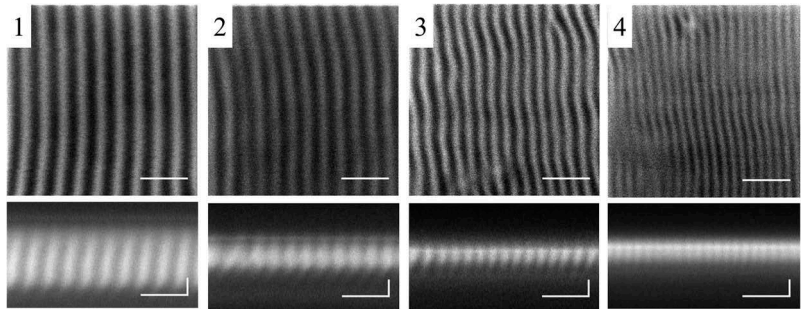

Figure 5. STED microscopy images of *xy* (above) and *xz* (below) cross-sections of N* mixtures with different pitch. In *xz* cross-sections cholesteric layers close to parallel with the *z* axis are observed, with interlayer distance of $\sim p/2$. The estimated thickness of the LC layer in these samples is between 500 nm and 1μm. Horizontal and vertical bars correspond to 500 nm.

microscope. Additionally, contrary to general impression, lateral resolution of ordinary optical microscopy with good index matching between the objective and the sample cover glass and with carefully selected narrow-band illumination is in our case quite superior to fluorescent confocal microscopy. The reason is in the wavelength of operation. Blue and near UV LED sources can be used for narrow-band illumination in ordinary microscopy, which gives us impressive experimentally achievable lateral resolution of ~140 nm. This is outperforming lateral resolution of the confocal fluorescent microscopy, which is operating in the red region of the visible spectrum and cannot resolve features bellow 300 nm. It is clear that resolution of fluorescent confocal microscopy could be improved by the design of blue fluorescent dyes, which could be excited in the UV spectrum. However, this results in other difficulties such as the limited spectral transmission window of commercial microscopes.

This work deals with comparison of lateral resolution of three different optical microscopy techniques in thin samples of CLCs. It is expected that STED microscopy is more vulnerable to optical effects in thick birefringent samples. Namely, the excitation and STED beam operate at different wavelengths and artefacts due to wavelength dispersion (colour) effects might be quite serious for STED microscopy in thick birefringent LC samples. Nevertheless, for specific optical studies of thin samples, such as for example topological defects in very thin layers, STED microscopy is definitely a strong technique, which could bring novel insight into structure and dynamics of defects on a nanometre scale.

Acknowledgments

We acknowledge Dr. David Wilkes, Merck KGaA for providing the cholesteric samples used.

Disclosure statement

No potential conflict of interest was reported by the authors.

Funding

This work was funded by Slovenian Research Agency (ARRS) through the contracts PR-08332 (J.P.) and P1-0099 (I.M., G.P.); Javna Agencija za Raziskovalno Dejavnost RS.

ORCID

J. Pišljar http://orcid.org/0000-0002-0349-2472

References

[1] Muševič I. Liquid crystal colloids. Cham, Switzerland: Springer International Publishing; 2017.
[2] Smalyukh I, Shiyanovskii SV, Lavrentovich O. Three-dimensional imaging of orientational order by fluorescence confocal polarizing microscopy. Chem Phys Lett. 2001;336:88–96.
[3] Wang X, Miller DS, Bukusoglu E, et al. Topological defects in liquid crystals as templates for molecular self-assembly. Nat Mater. 2015 Sep;15(1):106–112.
[4] Tai JSB, Smalyukh II. Super-resolution stimulated emission depletion microscopy of director structures in liquid crystals. Opt Lett. 2018 Oct;43(20):5158.
[5] Vitek M, Muševič I. Nanosecond control and optical pulse shaping by stimulated emission depletion in a liquid crystal. Opt Express. 2015 Jun;23(13):16921–16932.
[6] Smalyukh II, Lavrentovich OD. Three-dimensional director structures of defects in grandjean-cano wedges of cholesteric liquid crystals studied by fluorescence confocal polarizing microscopy. Phys Rev E. 2002 Nov;66(5):051703.
[7] Nowicka K, Bielejewska N, Kuczyński W, et al. Exploration of liquid crystal structures using fluorescent confocal polarizing microscopy. Phase Transitions. 2014 Oct;87(10–11):1073–1079.
[8] Smalyukh II, Pratibha R, Lavrentovich OD, et al. Free-standing films of twist grain boundary TGBA and UTGBC liquid crystals studied by fluorescence confocal polarizing microscopy. Liq Cryst. 2003 Aug;30(8):877–888.
[9] Smalyukh II, Lansac Y, Clark NA, et al. Three-dimensional structure and multistable optical switching of triple-twisted particle-like excitations in anisotropic fluids. Nat Mater. 2009 Dec;9(2):139–145.
[10] Chen BG, Ackerman PJ, Alexander GP, et al. Generating the Hopf fibration experimentally in nematic liquid crystals. Phys Rev Lett. 2013 Jun;110(23):237801.
[11] Posnjak G, Čopar S, Muševič I. Points, skyrmions and torons in chiral nematic droplets. Sci Rep. 2016 May;6:26361.
[12] Posnjak G, Čopar S, Muševič I. Hidden topological constellations and polyvalent charges in chiral nematic droplets. Nat Commun. 2017 Feb;8:14594.
[13] Posnjak G. Topological formations in chiral nematic droplets. Cham, Switzerland: Springer International Publishing; 2018.
[14] Webb RH. Confocal optical microscopy. Rep Prog Phys. 1996 Mar;59(3):427–471.
[15] Yeh P, Gu C. Optics of liquid crystal displays. New Jersey, USA: John Wiley & Sons; 2009.
[16] Varanytsia A, Posnjak G, Mur U, et al. Topology-commanded optical properties of bistable electric-field-induced torons in cholesteric bubble domains. Sci Rep. 2017;7:16149.
[17] Hell SW, Wichmann J. Breaking the diffraction resolution limit by stimulated emission: stimulated-emission-depletion fluorescence microscopy. Opt Lett. 1994 Jun;19(11):780.
[18] Westphal V, Hell SW. Nanoscale resolution in the focal plane of an optical microscope physical. Rev Lett. 2005 Apr;94(14):143903.

[19] Schermelleh L, Heintzmann R, Leonhardt H. A guide to super-resolution fluorescence microscopy. J Cell Biol. 2010 Jul;190(2):165–175.
[20] Sahl SJ, Hell SW, Jakobs S. Fluorescence nanoscopy in cell biology. Nat Rev Mol Cell Biol. 2017 Sep;18 (11):685–701.
[21] Schermelleh L, Ferrand A, Huser T, et al. Super-resolution microscopy demystified. Nat Cell Biol. 2019 Jan;21(1):72–84.
[22] Reynolds GA, Drexhage K. New coumarin dyes with rigidized structure for flashlamp- pumped dye lasers. Opt Commun. 1975;3(20):222–225.
[23] Pajk S, Majaron H, Novak M, et al. New coumarin- and phenoxazine-based fluorescent probes for live-cell STED nanoscopy. Eur Biophys J. 2019 Mar;48(5):485–490.
[24] Sednev MV, Belov VN, Hell SW. Fluorescent dyes with large stokes shifts for super- resolution optical microscopy of biological objects: a review. Methods Appl Fluoresc. 2015;3(4):042004.
[25] Merck, editor. Liquid crystal mixtures for electro-optic displays. In: Licristal technical brochure. Darmstadt (Germany): Merck KGaA, Liquid Crystals Division; 2002.
[26] Škarabot M, Lokar Ž, Gabrijelčič K, et al. Atomic force microscope based method of measuring short cholesteric pitch in liquid crystals. Liq Cryst. 2011 Aug;38 (8):1017–1020.
[27] Nych A, Fukuda J, Ognysta U, et al. Spontaneous formation and dynamics of half- skyrmions in a chiral liquid-crystal film. Nat Phys. 2017;13 (8):1215.
[28] Baudry J, Pirkl S, Oswald P. Topological properties of singular fingers in frustrated cholesteric liquid crystals. Phys Rev E. 1998 Mar;57(3):3038–3049.
[29] Voloschenko D, Lavrentovich OD. Optical vortices generated by dislocations in a cholesteric liquid crystal. Opt Lett. 2000 Mar;25(5):317.
[30] Shiyanovskii SV, Smalyukh II, Lavrentovich OD Computer simulations and fluorescence confocal polarizing microscopy of structures in cholesteric liquid crystals. In: Defects in liquid crystals: computer simulations, theory and experiments. Dordrecht, Netherlands: Springer; 2001. p. 229–270.